J Paleolimnol (2016) 55:1–16
DOI 10.1007/s10933-015-9853-3

ORIGINAL PAPER

A hydroclimate-proxy model based on sedimentary facies in an annually laminated sequence from Lake Ohau, South Island, New Zealand

Heidi A. Roop · Richard Levy · Gavin B. Dunbar · Marcus J. Vandergoes · Jamie Howarth · Sean Fitzsimons · Heung Soo Moon · Christian Zammit · Robert Ditchburn · Troy Baisden · Ho Il Yoon

Received: 28 January 2015 / Accepted: 12 August 2015 / Published online: 8 October 2015

Abstract Annually laminated sediments collected from Lake Ohau, New Zealand offer an opportunity to generate a high-resolution paleoclimate record for the Southern Hemisphere mid-latitudes. Correlation between regional precipitation and synoptic climate indices like the Southern Annular Mode, paired with a correlation between Ohau catchment precipitation, lake inflow and suspended sediment yield suggest that the Lake Ohau varves are a potentially powerful tool for estimating the amplitude, timing and interdependence of different climate modes operating in the Southern Hemisphere mid-latitudes over time. A robust chronology and sound climate-proxy model are fundamental requirements for all high-resolution paleoenvironmental records. Here we present a chronology derived from layer counts, and ^{137}Cs and ^{210}Pb ages for the top 60 cm of sediments from the distal basin of Lake Ohau that confirm the varved natured of the sedimentary sequence. Sedimentary facies of different varve motifs are used to develop a hydroclimate-proxy model which links stratigraphy to seasonal hydrology. To establish this relationship we use a model accuracy statistic, which shows a quantitative difference between the annual hydrographs associated with each of three primary varve motifs. Distribution of above average inflow events points to summer and autumn hydrologic regimes as the primary control on the deposition of different

Electronic supplementary material The online version of this article (doi:10.1007/s10933-015-9853-3) contains supplementary material, which is available to authorized users.

H. A. Roop (✉) · R. Levy · M. J. Vandergoes · J. Howarth · R. Ditchburn · T. Baisden
GNS Science, PO Box 30368, Lower Hutt 5040, New Zealand
e-mail: roop.heidi@gmail.com

R. Levy
e-mail: R.Levy@gns.cri.nz

M. J. Vandergoes
e-mail: M.Vandergoes@gns.cri.nz

J. Howarth
e-mail: J.Howarth@gns.cri.nz

R. Ditchburn
e-mail: R.Ditchburn@gns.cri.nz

T. Baisden
e-mail: T.Baisden@gns.cri.nz

H. A. Roop · G. B. Dunbar
Antarctic Research Centre, Victoria University of Wellington, PO Box 600, Wellington 6140, New Zealand
e-mail: Gavin.Dunbar@vuw.ac.nz

S. Fitzsimons
Department of Geography, University of Otago, 362 Leith Street, North Dunedin, Dunedin 9016, New Zealand
e-mail: sjf@geography.otago.ac.nz

H. S. Moon · H. I. Yoon
Korea Polar Research Institute, 26 Songdomirae-ro, Yeonsu-gu, Incheon 406-840, Korea
e-mail: jepy@kopri.re.kr

H. I. Yoon
e-mail: hiyoon@kopri.re.kr

motifs. This relationship between varve characteristics and hydrology will serve as a tool to reconstruct lake inflow, and by extension precipitation, on an annual basis throughout the late-Holocene for the South Island of New Zealand.

Keywords Varves · Southern Hemisphere · Hydroclimate · Stratigraphy · Complexity

Introduction

High-resolution paleoclimate records that capture environmental change on sub-decadal timescales play an important role in bridging the gap between short instrumental records and longer, lower resolution paleoclimate sequences (Zolitschka and Pike 2014). Only a few types of records capture environmental change at such high resolution. These include tree rings, ice cores, varved sediments, corals and speleothems (Bradley 1999; Zolitschka and Pike 2014). A number of these records are documented across the Northern Hemisphere (Mann et al. 2008; Ojala et al. 2012), but there remains a need to develop high-resolution paleoclimate reconstructions from the Southern Hemisphere (Neukom and Gergis 2012). New Zealand is one of only few landmasses that lie in the core of the climatically important Southern Hemisphere westerly wind belt but few high-resolution terrestrial paleoclimate records have been recovered from the North and South Islands (Page et al. 1994, 2010; Cook et al. 2002, 2006; Lorrey et al. 2008; Orpin et al. 2010; Augustinus et al. 2011; Fowler et al. 2012; Striewski et al. 2013). Sediment cores collected from distal end of Lake Ohau, South Island, New Zealand (Fig. 1) contain clastic varves, providing an opportunity to produce a high-resolution paleoclimate record from this important mid-latitude region (Roop et al. 2015).

Process-network studies of the climatic, physical and biological processes in contemporary lacustrine systems that are targeted for paleoclimate record development provide an important means by which the relationship between climate and core stratigraphy can be examined in detail and aid in the interpretation

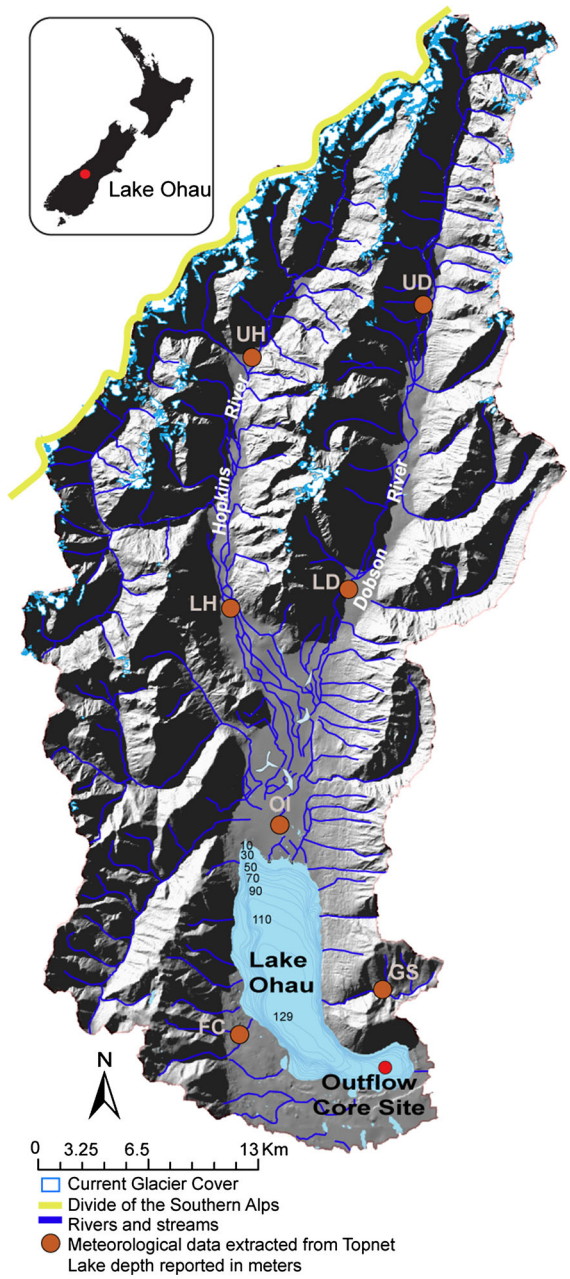

Fig. 1 The Lake Ohau catchment located on the eastern slope of the Southern Alps on the South Island, New Zealand. Sediment cores were collected near the lake outflow. Isobath interval is 10 m. Topnet derived precipitation time-series were generated for seven points in the Ohau catchment including: *UH* upper Hopkins, *UD* upper Dobson, *LH* lower Hopkins, *LD* lower Dobson, near the *OI* Ohau inflow, at the based of *FC* Freehold Creek and in the *GS* Greta Stream catchment

C. Zammit
National Institute of Water and Atmosphere,
PO Box 8602, Riccarton, Christchurch 8011, New Zealand
e-mail: Christian.Zammit@niwa.co.nz

and calibration of varved sediment sequences (Hodder et al. 2007; Ojala et al. 2012; Stockhecke et al. 2012; Lamoureux and Francus 2014; Zolitschka and Pike 2014). The Lake Ohau process-network study (ongoing) demonstrates that seasonal thermal stratification of the water column plays an important role in regulating the transfer of relatively coarser or finer grains from the river mouth to the distal (outflow) end of the lake (Fig. 1; Roop et al. 2015). Sediment accumulation in winter at the outflow is limited to very fine silt particles (3–5 μm) as cold, turbid underflows originating at the delta do not transport coarser silts and sands upslope beyond the depocentre. Increased discharge and sediment flux, paired with pronounced thermal stratification in summer, enables transport of fine silt particles (8–13 μm) to the core site along pycnoclines in the upper portions of the water column (Roop et al. 2015). These observations provide a clear mechanism for the deposition of annual laminations, or varves, in the contemporary system (Roop et al. 2015).

This study builds on this physical process study to describe and explain seasonal controls on sedimentation in Lake Ohau beyond the process-network monitoring period (2011–2013) discussed in Roop et al. (2015) and aims to: a) confirm that sediment laminations preserve a seasonal signal over the instrumental record (1900–2011), and; b) investigate the hydroclimatic and sedimentological variability over the instrumental record in order to establish a sound climate-proxy relationship. This work will serve as the primary tool for interpreting paleoclimate variability in an approximately 17,000-year record (~70 m) expected to be collected from Lake Ohau in mid-2016.

Study site

Lake Ohau (44.234°S, 169.854°E; 520 m asl) is a temperate lake (mean winter air temperature 6.2 °C) located in the intermontane Mackenzie Basin, South Island, New Zealand (Fig. 1). This glacially formed lake is 54 km^2 and reaches a maximum depth of 129 m. The 924-km^2 Ohau catchment ranges from 520 to 2640 m asl and is drained primarily by the Hopkins and Dobson Rivers (Fig. 1). The catchment geology is characterized by highly indurated quartzofeldspathic greywacke sandstone and argillite mudstone (Cox and Barrel 2007). The Hopkins and Dobson valleys have relatively small glaciers at their head, which over the instrumental period occupy approximately 1.7 % of the total catchment area (Fig. 1; Anderton 1973). This small volume of glacial ice is considered to have remained stable over the last several thousand years based on recent glaciological investigations in the valley (Doughty et al. 2013; Putnam et al. 2013) and is assumed to play a minor role in sediment generation and flux in the contemporary lacustrine environment (Roop et al. 2015).

The Hopkins and Dobson Rivers account for 85 % of the total fluvial input into Lake Ohau, with smaller tributaries contributing the remaining 15 % (Fig. 1; Woods et al. 2006). Precipitation and river inflow is highest during austral summer (average inflow 105 $m^3\ s^{-1}$) and lowest in winter (61 $m^3\ s^{-1}$; Roop et al. 2015). Spring and early summer snowmelt contributes approximately 21 % of mean annual inflow (Kerr 2013). Total monthly headwater precipitation and lake inflow are correlated (1994–2013; $r = 0.74$, $p = < 0.0001$). There is a strong precipitation gradient over the 37 km long catchment, with headwaters receiving 76 % more precipitation than at the lake (Roop et al. 2015). This gradient is the result of westerly wind driven orographic precipitation on the western side of the Southern Alps 'spilling over' the main divide into the upper part of the Ohau catchment (Chater and Sturman 1998; Salinger and Mullan 1999). Lake Ohau is seasonally stratified and experiences frequent overturning during the austral summer (October–March; Roop et al. 2015).

Materials and methods

Three short gravity cores (0.3 m) and three longer Mackereth cores (5.5 m; Mackereth 1958) were recovered near the outflow of Lake Ohau at ~68 m water depth between July 2009 and May 2013 (Fig. 1). Gravity cores were used to recover the sediment–water interface. The cores discussed in this paper include Mackereth cores OH1m1 (1 m; collected July 2009), OH6m1c (5.5 m; collected October 2012), OH6m1 (5.5 m; collected July 2009), and gravity core GCS_1 (0.23 m; collected May 2013).

Physical properties

Density, compressional (p)-wave velocity, magnetic susceptibility (whole core), and line scan RGB data

(split core) were collected from cores OH6m1c, OH1m1, and OH6m1 using a Geotek multi-sensor core logger at the University of Otago. GCS_1 was split and photographed using a Lumix 10.1 Megapixel DMC LX5 camera. Thin-sections from core OH6m1 were made following Lamoureux (1994) and scanned at 2400 dpi on a flatbed scanner. X-radiographs (X-rays) were acquired from 30 cm × 0.5 cm × 0.5 cm u-channel samples taken from OH6m1c (Fig. 2a). Each u-channel sub-sample was offset with an overlap of 1.5 cm. X-ray data were collected at twenty-micron resolution using an ITRAX^{TM} core scanner housed at the Korea Polar Research Institute (KOPRI). X-rays were generated using a 3 kw Mo tube running at 40 kV and 35 mA with scanning time of 500 ms. Greyscale data were extracted from 16-bit X-ray positive (where lower density is represented by a lighter tone) TIFF images generated by the ITRAX^{TM} using ImageJ (Schneider et al. 2012). Images were adjusted for brightness and contrast to fit within a range of intensity between 33,000 and 36,500.

Particle size was measured on selected high and low-density laminae from GSC_1 to verify that density variation is primarily due to changes in particle-size-influenced porosity (ESM1). Discrete samples were pretreated with 27 % H2O2 to remove the organic component (3.2 %; Roop et al. 2015), dispersed with sodium hexametaphosphate (Calgon), continuously stirred and sonicated for 30 min, and passed through a Beckman Coulter LS 13 320 laser diffraction particle size analyzer equipped with a Micro Liquid Module (MLM). The MLM is capable of measuring small (~0.03 g) samples, ensuring material from lamina <2 mm thick could be obtained. Particle size data statistics were generated using Gradistat software (Blott and Pye 2001).

Chronology

One-centimeter sections extracted at various depths from core OH1m1 were analyzed for both ^{137}Cs and ^{210}Pb activity (ESM2). ^{137}Cs was measured directly by gamma spectrometry using a high-resolution low background germanium (well-crystal) detector and total ^{210}Pb was determined from its granddaughter ^{210}Po measured by alpha spectrometry. Unsupported ^{210}Pb was calculated from the total by subtracting supported ^{210}Pb, estimated by measuring ^{226}Ra using gamma spectrometry. All analyses were conducted at GNS Science, New Zealand. The CRSmodel program, which assumes a Constant Rate of Supply (CRS), was used to determine the ^{210}Pb age-depth relationship (https://code.google.com/p/crsmodel/, accessed Nov 19, 2014; Fig. 2). Correlation between OH1m1 and

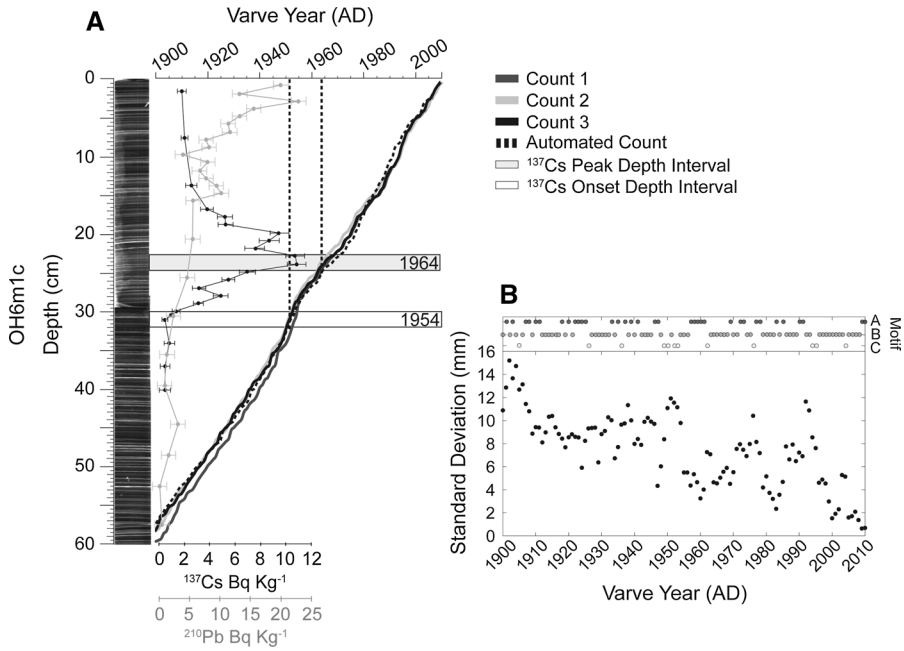

Fig. 2 **a** ^{137}Cs and ^{210}Pb activity profiles compared to manual operator and automated counts for the top 60 cm of core OH6m1c. All counts are consistent with the depth intervals associated with the 1964 peak in ^{137}Cs and onset of ^{137}Cs in the early 1950s. **b** 1σ standard deviation for all manual and automated counts compared to three described motifs. The maximum deviation is 15.2 mm or ±2.9 years based on the ^{137}Cs-derived sedimentation rate. The greatest deviation between counts is associated with motif C, or event stratigraphy

OH6m1c was conducted visually in Corelyzer (http://andrill.org/~jareed/corewall.org/www/) and indicated an average ~1 cm offset between the cores for the top 60 cm (ESM2). The offset is a result of the difference in the year of core collection and disturbance of the surface from coring. For example, gravity core GCS_1 and OH6m1c (recovered with a Mackereth system) were both collected in 2012. Correlation between these two cores shows that two full laminations were lost in the Mackereth core, which means that the surface of OH6m1c represents varve year 2010.

Layer counting

Based on our studies of modern sedimentation processes, the coarse–fine couplets are interpreted as annual layers and were counted accordingly. Three layer counts were generated by two independent operators (HR, RL) from a combination of X-ray images, line-scan images, and thin sections for the top 60 cm of OH6m1c and OH6m1 (Fig. 2a). Each operator assigned a 'varve year' (VY) to each couplet based the occurrence of a sharp density change and a visual change in particle size in thin section. HR conducted two separate counts. An objective method was used to generate layer counts which places the end of a nominal year wherever a positive gradient equivalent to ~20 % of the total amplitude occurred within a 0.5-mm interval (Wheatley et al. 2012). We also assumed that annual sediment accumulation must be >2 mm based on prior monitoring (Roop et al. 2015), so concurrent greyscale peaks that were <2 mm apart were not counted as separate years but classified as sublaminae. The resulting layer counts are shown in Fig. 2. Sedimentation rate and layer thickness versus year are derived from these age-depth relationships. Because the major coarse layer in the sedimentary couplet is the easiest feature to identify in the greyscale record and is caused by an influx of sediment in spring, a varve year is defined as September 1st–August 31st (which differs slightly from Roop et al. 2015 who defined a VY as October 1st–September 31st). This modification enables an investigation of variability in spring inflow conditions.

Hydrometeorological data

Three hydrometeorological datasets were used in this study including: (1) a record of daily mean inflow calculated from lake level and measured outflow that extends from 1926 to present (Meridian Energy Ltd., unpublished data); (2) a continuous time-series of precipitation and temperature (1926-present) measured at Lake Tekapo Air Safaris, 40 km north of Lake Ohau and outside of the Ohau surface water catchment (44.00°S, 170.43° E; 762 m asl; Station ID 4970); and (3) modeled precipitation, air temperature and inflow data extracted for seven different locations in the Lake Ohau catchment from the National Institute of Water and Atmosphere (NIWA) Topnet model (Clark et al. 2008; Fig. 1). Topnet is based on a 30-m Digital Elevation Model (DEM) and simulates hydrological processes based on total precipitation and temperature provided as a 0.05° latitudinal/longitudinal grid based on an interpolation of data from a national network of automated weather stations (Tait et al. 2006). The hydrological model was calibrated against hourly total lake inflows over the period 1980–1990 (Nash–Sutcliffe = 0.779) and validated over the period 1980–2008 (Nash–Sutcliffe = 0.777). Seven samples sites were selected to provide upstream catchment average precipitation and temperature and total inflow, including: Upper Hopkins (UH), Upper Dobson (UD), Lower Hopkins (LH), Lower Dobson (LD), near the Ohau inflow (OI), at the base of Freehold Creek (FC) and in the Greta Stream catchment (GS; Fig. 1).

Comparisons between varve thickness (VT) and hydrometeorological data were run for seven different temporal increments including: full 12 months, spring (September, October, November, referred to as SON), summer (December, January, February, referred to as DJF), autumn (March, April, May, referred to as MAM), winter (June, July, August, referred to as JJA), spring & summer (SONDJF), and autumn & winter (MAMJJA). Averages and totals of the three hydrometeorological datasets over these temporal increments were tested against the full VT time-series and all varve motifs and sub-types for five different varve features including: (1) total thickness; (2) coarse unit thickness; (3) fine unit thickness; (4) fine unit thickness minus sublaminae; (5) sublaminae thickness. Lag correlations between VT characteristics and hydrometeorological parameters were also tested for the preceding one and 2 years. All statistical relationships between each measured varve feature and hydrometeorological variables were tested using Spearman's rank correlation (non-parametric) as all datasets were

non-normally distributed. Relationships where $p \leq 0.05$ are considered significant.

Varve year hydrographs were compared using the Nash–Sutcliffe model accuracy statistic (Nash and Sutcliffe 1970). The Nash–Sutcliffe coefficient tests values for goodness of fit between measured and modeled hydrographs. The goodness of fit, represented here as r, is analogous to the sum of squares, where 1 is a perfect fit and values ≤ 0 indicate that the model hydrograph is a poor predicator of the measured discharge values compared to the average discharge over the period considered. In this study, the Nash–Sutcliffe coefficient was used to compare the mean of measured hydrographs for differing varve motifs and types. Annual and seasonal hydrographs for each primary sedimentary motif were also compared using the Spearman's rank correlation.

Results

X-ray density and particle size

Sedimentation patterns in Ohau are dominated by a signal comprised of a coarse and fine couplet, represented in greyscale by high ($\sim$35,000–36,500) and low intensity values ($\sim$33,000–35,000), respectively (Fig. 3). This dominant pattern is often overprinted by the occurrence of additional coarse sublaminae (greyscale intensities of $\sim$34,000–36,000), as observed by Roop et al. (2015). The less dense layers (light grey and white tones in X-rays) are consistently associated with coarser particles (modal size >8.0 μm), while the densest layers (dark tones in X-rays) are associated with finer particles (modal size 3.7 μm; ESM1). Particle size variability between the light and dark layers in X-ray is similar to the annual range measured in surface cores and sediment traps by Roop et al. (2015).

Varve classification

Three primary varve motifs (labeled A, B and C) were identified based on variations in complexity (e.g. presence/absence and number/position of sub-laminae) and total thickness (Table 1; Fig. 3). Motif A consists of a fine silt basal layer that grades into a very fine silt layer. These 'simple' varves are divided into sub-types A1 and A2, which are separated based on the relative thickness of the coarse (fine silt) and fine units (very fine silt; Table 1; Fig. 3). Motif A accounts for 34 % of the total lamination stratigraphy in the top 60 cm of OH6m1c. Motif B is characterized by the presence of one or more grain-supported 0.5–1.5 mm-thick sublaminae within the primary coarse/fine stratigraphy. These 'complex' varves account for 56 % of the total lamination stratigraphy in the top 60 cm of OH6m1c. Motif B is sub-divided into four types (B1, B2, B3, B4) to account for the variations in the number and position of sublaminae within the annual couplet (Table 1; Fig. 3). Motif C includes layers that are $\geq$9.0 mm thick and comprise a basal fine silt layer that grades into a relatively thick ($\sim$3.5 mm) homogeneous very fine silt layer (Table 1; Fig. 3). Thin sub-laminae ($\leq$1.0 mm) commonly occur immediately above the basal unit. Motif C accounts for 10 % of the varve stratigraphy in the top 60 cm of OH6m1c. Total VT ranges from 3.4–3.5 mm in Motif A, 4.5–7.1 mm in Motif B, and 9.0–12.9 mm Motif C (Table 1; Fig. 3).

Core chronology

Cesium-137 and lead-210 radiometric dating techniques and layer counts provide both a robust age-depth model for the instrumental record and a method to test whether the lamination stratigraphy preserves an annual signal. Southern Hemisphere onset and peak ^{137}Cs fallout, a by-product of nuclear weapons testing, occurs in 1954 and 1964, respectively (UNSCEAR 2000). These tie-points offer important age-control for the top portion of the sediment record. Peak ^{137}Cs (1964) occurs between 24.0 and 25.0 cm and onset (1954) occurs between 31.0 and 32.0 cm in OH6m1c (ESM2).

Chronology determined by layer counts (manual and automatic) is consistent with the depth intervals associated with the ^{137}Cs profile (Fig. 2a). Specifically, layer counts place varve year (VY) 1964 between 23.7 and 24.8 cm and VY 1954 between 28.8 and 30.5 cm. Similar sediment accumulation rates (SAR) are calculated using ^{137}Cs and ^{210}Pb activity profiles and layer counts (Fig. 2a). The ^{137}Cs derived SAR is 5.1 $\pm$ 0.3 mm year^{-1}, the ^{210}Pb SAR is 6.0 $\pm$ 1.1 mm year^{-1} and the layer count derived SAR is 5.2 $\pm$ 0.5 mm year^{-1}. The instrumental record commenced in 1926 and the ^{210}Pb-derived and layer counts age-depth relationships are in close

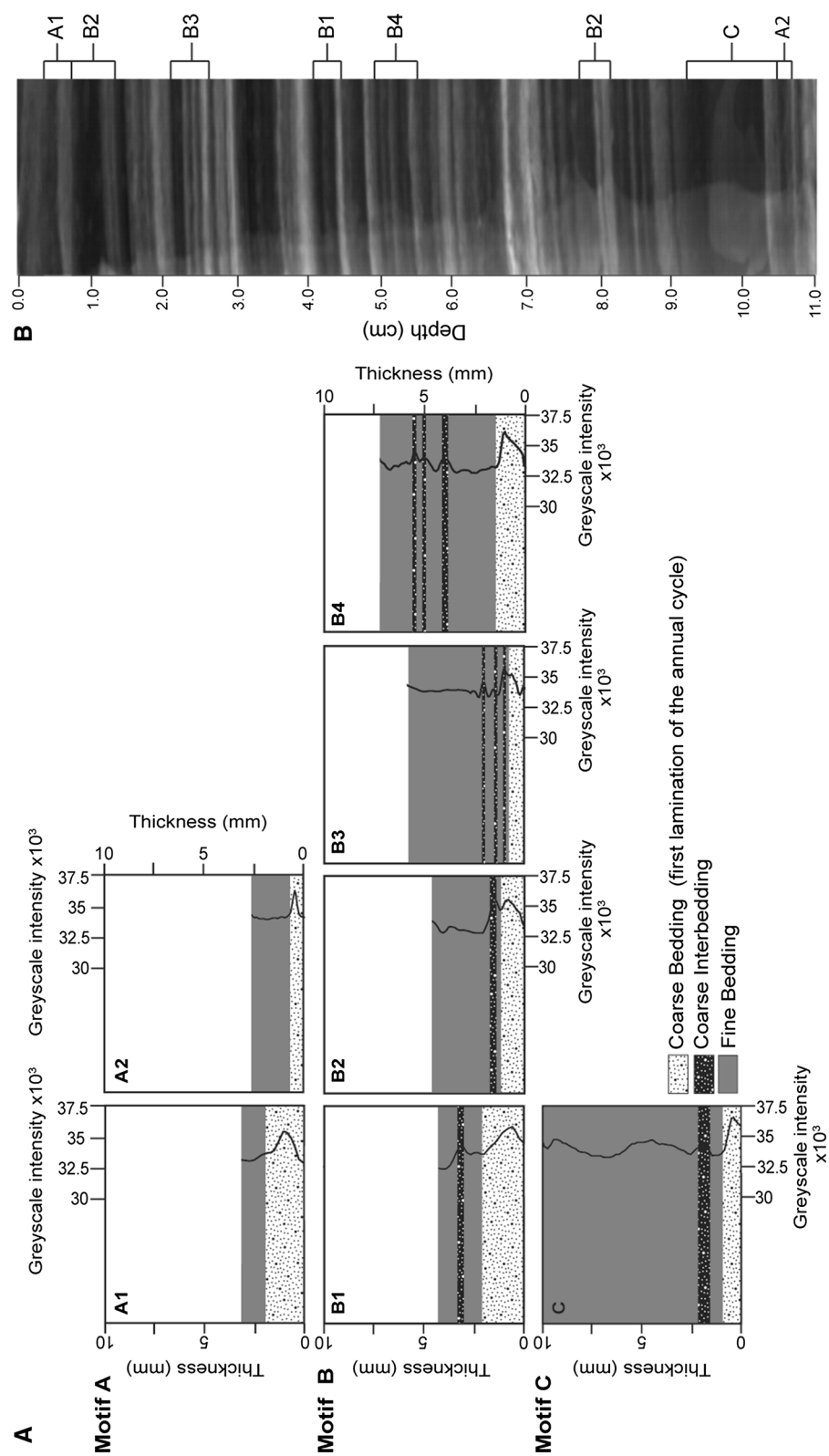

Fig. 3 **a** An example of the differing stratigraphic patterns and greyscale curve for each of the seven different varve types characterized by motifs A, B, C. Each example shows the relative thickness of each unit and the presence and stratigraphic position of sublaminae in motifs B and C. Unit thickness is based on the mean of each varve type. **b** X-radiograph image with an example of each varve sub-type

Table 1 Varve classification for the different varve motifs and sub-types

Description	Mean thickness (mm)	Mean coarse unit Thickness (mm)	Mean fine unit thickness (mm)	Mean number of sublaminae	Occurrence[a] (%)	Interpretation [note: spring (SON); summer (DJF); autumn (MAM); winter (JJA)]
Motif A—defined by a coarse/fine couplet lacking sublaminae						
A 1 Composed of fine silt basal layer grading into a very fine silt layer. Silt layer is thicker than very fine silt layer. Contains no sublaminae	3.5	2.0	1.5	0	7	Simple varve dominated by spring discharge
A 2 Composed of silt basal layer grading into a very fine silt layer. Fine silt layer is thicker than the silt layer. Contains no sublaminae	3.4	1.1	2.3	0	27	Simple varve dominated by late spring discharge
Motif B—defined by coarse/fine couplet with one or more coarse sublaminae						
B1 Composed of fine silt basal layer grading into a very fine silt layer. Very fine silt layer contains one coarse-grained <1.5 mm thick sublaminae	4.7	1.2	1.6	1	19	Complex annual hydrograph; spring-dominated signal with late season inflow event
B2 A fine silt basal layer grades into the very fine silt layer. <1.0 mm fine silt sublaminae are present proximal (<0.8 mm) to the fine silt basal layer. Sublaminae are not present near the top of the very fine silt unit	4.8	1.1	2.2	1	12	Complex annual hydrograph; dynamic spring hydrograph with late spring/early summer peak inflow event
B3 A fine silt basal layer grades into the very fine silt layer. One or more <1.0 mm fine silt sublaminae are present proximal to the fine silt basal layer. Sublaminae are not present near the top of the very fine silt unit	5.6	0.9	1.7	2	9	Complex annual hydrograph; numerous peaks in summer discharge
B4 Composed of fine silt basal layer grading into a very fine silt layer. Very fine silt layer contains several fine silt <1.0 mm thick sublaminae	7.1	1.1	2.1	3	16	Complex annual hydrograph; numerous peaks in summer and autumn discharge
Motif C—defined by graded coarse deposits overlain by a (≥3.5 mm) *fine unit. Total unit thicknesses >9.0 mm*						
C1 Composed of a basal silt layer which grades into a thick (>3.5 mm) non-graded fine silt layer. Sublaminae are common in basal layer	10.0	1.5	3.4	2	10	Event layer; large summer discharge exceeding ~880 $m^3 s^{-1}$

[a] Percent occurrence since 1900 AD based on varve counts

agreement; ^{210}Pb places 1926 (±6.1 years) at 44.0–45.0 cm while an average layer count places 1926 (±2 years) at 44.5–45.0 cm.

A 1σ of the ages assigned to a given depth is used as a means to quantify offset between the four different layer counts (three manual and one automated; Fig. 2b). A maximum deviation of 15.2 mm or ±3 years occurs at VY 1900. The largest deviation between counts generally occurs in sections of the core that are characterized by motif C and the total error then propagates with depth (Fig. 2b). Maximum agreement and consistency between layer counts occurs in sections that are characterized by motif A. Given the similarity and small error between the layer count- and radiometric-derived age-depth relationships, hydroclimatic relationships over the instrumental record were tested against an average of the manual and automated layer counts.

Hydroclimate-varve relationships

Regression statistics were calculated to compare the thicknesses of the five possible components of each varve (e.g. total thickness, coarse unit thickness, fine unit thickness, fine unit thickness without sublaminae, sublaminae thickness) with average modeled air temperature, areal total and average modeled and measured precipitation, and total and average inflow for the seven different temporal/monthly breakdowns of the annual cycle. These tests carried out using the instrumental record (1926–2010) yield few statistically significant results (ESM3). One of the strongest correlations over the instrumental period is a basin-wide negative correlation between total SON precipitation and coarse unit thickness. This correlation is weakly significant for six of the seven sites for which modeled precipitation was extracted; the strength of the correlation only ranges from $r = -0.29, p = 0.08$ at Freehold Creek (FC) to the strongest correlation of $r = -0.36$, $p = 0.03$ at Greta Stream (GS). The correlation is not significant for the Upper Hopkins site. The same regression statistics were tested on the different three major varve motifs and seven types, which yielded similar non-robust and weakly statistically significant results (ESM3).

In order to explore the relationship between varve motif/type and hydroclimate, each annual layer was correlated with its corresponding hydrograph (derived from the Lake Ohau inflow time-series (1926–2010) provided by Meridian Energy Ltd.) To mitigate the impact of potential mismatches between varve type and hydrology arising from errors in our annual layer chronology, we compared hydrographs for a subset of years of close chronologic sequence (1–5 sequential years) defined by each motif and varve type (Table 2). The annual inflow time-series for the subsets of years corresponding to motifs A, B, C and varve types A1, A2, B1, B2, B3, B4, C respectively, were grouped and averaged to produce a characteristic hydrograph for each motif and type (Fig. 4). These characteristic hydrographs were then compared using the Nash–Sutcliffe model accuracy statistic and Spearman's rank correlation (Tables 2 and 3; Nash and Sutcliffe 1970).

Comparisons between each characteristic (mean) hydrograph for the subsets of years were made using a complete data series and both a 30- and 15-point running mean (Fig. 4). Results from analysis of the 15-pt smoothed data series for the subset of chronologically sequential varves ($n = 5$ or 6) show poor fit between the hydrographs that characterize motif A and C and close agreement between those that characterize motifs B and C (Table 2). Hydrographs for subtypes A1 and A2 are in close agreement with B1 and B2 (Table 2). To increase the statistical power of the correlations, hydrographs for the sum of all of the years represented by each of the three major motifs were also compared (minimum $n = 11$ for motif C). The strong positive correlation between the subset of annual hydrographs (15-pt smooth) for all motifs weakens significantly when weekly data are considered (Table 3).

To explore seasonal biases in inflow, characteristic hydrographs for the major motifs and types were divided into four temporal increments including: spring (SON), summer (DJF), autumn (MAM), and winter (JJA) and compared using a Spearman's rank correlation and outlier plots (Table 4; Fig. 5). The hydrographs for each motif during SON show close correlation while the relationship between the seasonal hydrologic regimes and varve motifs weakens for the rest of the annual cycle (Table 4). Outlier plots show similar patterns for all of the varve types, but with the range of hydrologic variability the lowest during JJA. The number of hydrologic outliers increases most notably in summer and autumn (Fig. 5). Outliers in seasonal discharge are mostly associated with motif B varve types, while type A

Table 2 Nash–Sutcliffe coefficients (r) for 15-point smooth hydrographs

Mean hydrographs are derived from the listed subset of years. Sequential years were selected, where possible, in order to minimize potential error associated with the varve chronology. For type A1, no chronologic sequence of years was available for testing. Hydrographs are derived from the Lake Ohau inflow time-series

Varve type	A1	A2	B1	B2	B3	B4	C1
A1	1	0.54	0.70	0.56	0.40	0.40	0.45
A2	0.54	1	0.50	0.72	0.50	0.50	0.47
B1	0.70	0.5	1	0.69	0.45	0.68	0.62
B2	0.56	0.72	0.69	1	0.50	0.37	0.61
B3	0.40	0.50	0.45	0.50	1	0.30	0.61
B4	0.40	0.50	0.68	0.37	0.30	1	0.26
C1	0.45	0.47	0.62	0.61	0.61	0.26	1
Years compared	2009	1973	1968	2008	1980	1999	1995
	1991	1972	1966	2005	1979	1996	1994
	1977	1961	1965	2001	1975	1993	1953
	1958	1960	1964	1948	1956	1932	1952
	1947	1959	1963	1945	1954	1930	1950
	1939			1943		1929	1949

varves show the smallest range of variability across the annual cycle, and the fewest number of anomalous peaks in inflow (Fig. 5).

Discussion

Meaningful paleoclimate reconstructions from annually laminated sediments require a detailed understanding of the relationship between sedimentation and climate (Hodder et al. 2007). In the Lake Ohau region, there is significant correlation between totally monthly headwater precipitation and lake inflow ($r = 0.74$ $p = < 0.0001$), as well as inflow and fluvial sediment yield for South Island greywacke catchments ($r = 0.71$; Hicks et al. 2011; shown here as r, a correlation coefficient). This regional relationship suggests there should be a link between rainfall and sediment accumulation in Lake Ohau. The original hypothesis was that this link would be reflected in VT based on previous paleoclimatic reconstructions in many clastic varve settings (Desloges and Gilbert 1994; Tomkins and Lamoureux 2005; Kaufman et al. 2011). However, results indicate that such a relationship does not exist at Lake Ohau. This is not entirely surprising as direct relationships between VT and hydroclimatic variables can be difficult to establish (Hodder et al. 2007). Geologic processes such as earthquakes and slope failure can, in geologic time, instantly alter the sediment availability of a basin (Dadson et al. 2004; Howarth et al. 2012). The climate system itself operates on various temporal and spatial scales and can be complicated in mountainous terrain by microclimates, which are poorly resolved in modeled data and generally underrepresented in meteorological time-series (Hannah et al. 2000). In addition to the aforementioned complexities, internal lake dynamics can further attenuate dispersal and accumulation patterns of sediments (Pharo and Carmack 1979; Desloges and Gilbert 1994; Hodder et al. 2007). Regardless of these complexities, our results suggest that varve stratigraphy, instead of varve thickness, is a good indicator of hydroclimatic variability in Lake Ohau. In the following discussion we explore the probable causes of stratigraphic variability and show that varve stratigraphy can be used to establish a hydroclimate-proxy model.

Varve thickness and hydroclimatic variability

A strong correlation between suspended sediment yield and inflow has been shown for nearby catchments (Hicks et al. 2011) and a similar relationship is assumed to be true for Lake Ohau. However, the predominance of negative correlations between total precipitation, inflow and varve thickness at Lake Ohau (ESM3) suggests that sediment accumulation and inflow are decoupled due to seasonal lake hydrodynamics. Specifically, inflow events in spring occur when the lake is isothermal, which influences sediment transport pathways and affects the relationship between inflow (discharge) and suspended sediment flux (Roop et al. 2015). Furthermore, errors in sediment flux derived from suspended sediment concentration (SSC) rating curves can be in excess of 50 % and tend to produce

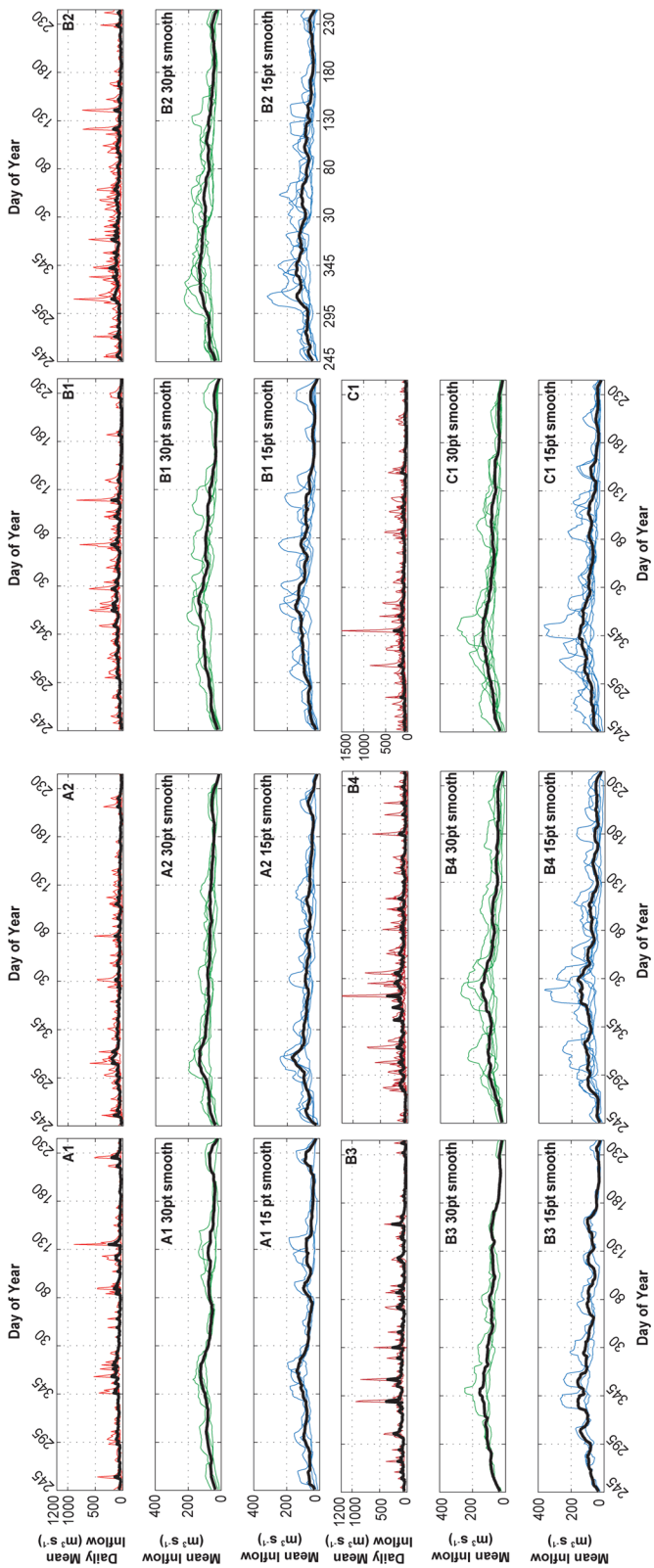

Fig. 4 Plots showing the full, 15-point and 30-point smoothed hydrographs for each motif sub-type. Dark bold lines are the mean of all years in each comparison (Table 2). Motif A varves are characterized by a spring season dominated hydrograph, motif B varves are characterized by a more complex hydrograph displaying a high degree of variability throughout the annual cycle. Motif C is similar to B, but is characterized by extreme summer event flows. Each of the three motifs is significantly different based on the Nash–Sutcliffe model accuracy statistic (Table 3)

Table 3 Nash–Sutcliffe coefficients (r) for the weekly smoothed annual hydrograph for each of the three major sedimentary motifs

Motif	A	B	C
A	1	−0.27	−0.46
B	−0.27	1	0.32
C	−0.46	0.32	1
n	22	52	11

The hydrograph for each motif is derived from a mean of all of the years characterized by each sub-type (e.g. A1, A2 = A). Each motif is characterized by a unique hydrologic regime

low estimates during high SSC conditions and vice versa (Walling and Webb 1988; Horowitz 2003). This demonstrates that relationships between inflow and SSC, and subsequent sediment transport and deposition, are complicated and cannot be assumed to be linear or constant through time.

Eight high magnitude (≥880 m^3 s^{-1}) inflow events were measured between 1926 and 2011 and eleven ≥9.0 mm laminations (motif C layers) were identified in the cores during the same period. Further, only fifty percent of layers characterized as motif C coincide temporally (±2 years) with measured high magnitude

Table 4 Regression statistics (r) for the seasonal mean hydrology of each of the three major motifs (for all years, as in Table 3)

Correlation between the three motifs is greatest in the spring (SON)

Motifs compared	Season			
	SON (spring)	DJF (summer)	MAM (fall)	JJA (winter)
A–B				
r	0.53	0.18	0.15	0.26
p value	<0.0001	<0.0001	<0.0001	<0.0001
A–C				
r	0.35	0.23	0.02	0.02
p value	<0.0001	<0.0001	0.21	0.30
B–C				
r	0.62	0.17	0.02	0.17
p value	<0.0001	<0.0001	0.17	<0.0001

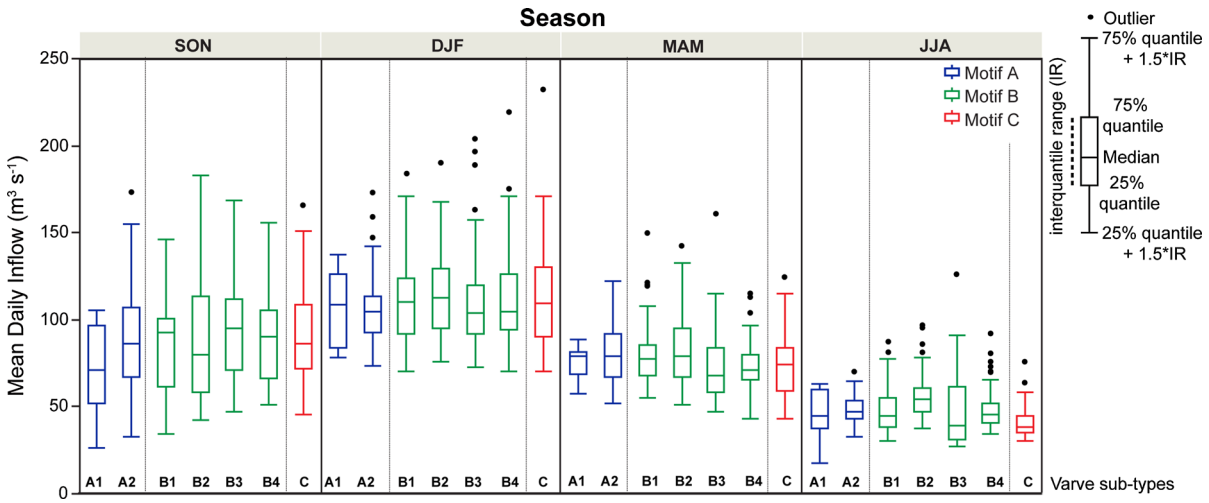

Fig. 5 Outlier box plots organized by season for each of the varve types. The hydrographs used for this comparison are derived from a mean of all of the years characterized by each varve type. Outliers represent anomalous flow, or event flow. A higher density of inflow events, particularly in summer and autumn, characterizes motif B

inflow peaks. This mismatch suggests that some large sedimentation events are potentially related to non-climatic events including subaqueous mass wasting. These observations are not surprising, as other studies have shown that peaks in SSC do not always correlate with peak inflow (Sawada and Johnson 2000; Orwin and Smart 2004). In addition, unusually dry conditions and associated high soil infiltration capacity can attenuate the sediment transport response following extreme precipitation events and affect expected SSC (Favaro and Lamoureux 2014). One or more of the processes outlined above could explain the observed mismatch between thick event layers and precipitation-driven extreme event inflow and the anti-correlation between precipitation, inflow and varve thickness.

Lamination stratigraphy

Sedimentary couplets with no sublaminae (motif A) represent varves that form in years with limited high magnitude summer/autumn inflow events (Figs. 4, 5). A1 varves form during years that are characterized by an annual hydrograph with a late-spring onset of high inflow that peaks in December/January and exhibits limited spring freshet input (Figs. 4, 5). This late season flux may account for the proportionally thicker coarse unit in A1 as peak flow occurs when the lake is fully stratified, which may provide a more direct conduit for coarser sediment delivery to the distal basin. A2 varves form during years characterized by a hydrograph exhibiting higher peak inflow in spring when lake stratification is developing, which may cause flow separation that delivers less sediment to the distal basin and produces the proportionally thinner basal coarse unit (Fig. 4). This interpretation may also explain the basin-wide negative correlation between coarse unit thickness and total SON precipitation. High spring rain may prolong isothermal conditions in the lake through the continued input of relatively colder precipitation and snowmelt. More persistent isothermal conditions could potentially limit the transport of coarse particles at the core site and produce thinner coarse basal units. Overall, the lack of complexity in motif A is likely associated with the smaller number of peak inflow events in summer and autumn (Fig. 5).

Sedimentary couplets that contain sublaminae characterize motif B. Sediment grain size in the basal layer of each sublamination is similar to the primary spring/summer coarse unit, which suggests that these units are deposited during inflow events of similar magnitude that occur between October and May when the lake is fully stratified (Roop et al. 2015; Fig. 4). However, we suggest that the thinner units reflect lower total suspended sediment flux due to lower total inflow volume or duration. Sublaminae in motif B are similar to those documented in other records with complex lamination stratigraphy (Desloges and Gilbert 1994; Chutko and Lamoureux 2008; Cockburn and Lamoureux 2008) and reflect short-lived summer and autumn rain events. This interpretation is consistent with Roop et al. (2015), who observed discrete sublaminae deposited during summer inflow events and captured in sediment traps at the Outflow site. Further, each sub-type of motif B includes several outliers in discharge during the stratified period in the summer and autumn (Fig. 5), which are likely responsible for producing the sublaminae characterizing motifs B and C. Type A2 is an exception, as it lacks sublaminae but has a summer hydrologic regime that includes numerous outliers in summer discharge; these peaks in inflow may be responsible for the proportionally thicker fine unit in A2 (compared to A1) and the lack of sublaminae potentially associated with internal lake dynamics.

Motif B is subdivided into four sub-types based on the position and thickness of sublaminae. The stratigraphic position of the sublaminae may, in general, reflect the position of summer and autumn inflow events within the annual hydrograph (Fig. 4). For example, sub-type B2 includes sublaminae that occur within the lower portion of the primary fine unit and has a characteristic hydrograph that is dominated by high magnitude spring and summer peaks in inflow (Figs. 4, 5). In contrast, sub-type B1 includes sublaminae that occur within the upper portion of the primary fine unit and is characterized by a hydrograph with a greater concentration of peak inflow events in the autumn (Figs. 4, 5).

Motif C is comprised of a thick fine (dense) unit that includes sublaminae thicker than those observed in motif B. This stratigraphy suggests that these varves form in years that include extreme inflow events. These extreme event flows generally range between 880 and 1300 $m^3 s^{-1}$ and can deposit sediment at nearly double the average annual sedimentation rate (Roop et al. 2015).

One annual hydrograph with a large (1200 $m^3 s^{-1}$) peak inflow event correlates with motif sub-type B4

(Fig. 4) and highlights that misclassification can occur. However, general agreement between the Nash–Sutcliffe correlation and regression statistics show that all three major motifs, and sub-types, are characterized by unique annual hydrologic regimes (Fig. 4; Table 3). High correlation between spring discharge and varve motif (and sub-types) suggests that the primary hydrologic causes for the different varve types occurs in summer and autumn. During summer and autumn, characteristic hydrographs for motifs B and C contain significant outliers in discharge (Fig. 5), which produce complex laminae. Furthermore, general agreement between the concentration and stratigraphic position of sublaminae and the number and timing of anomalous summer-autumn inflow events (outliers) suggests that stratigraphic pattern and hydrodynamics are closely related. Monitoring data through winter (JJA) showed that isothermal conditions prohibit the transport and deposition of coarse material to the Outflow (Roop et al. 2015). Therefore, changes in varve stratigraphy are interpreted as variations in the number and intensity of peak inflow events during the summer and autumn seasons. Specifically, the three primary motifs are interpreted to represent the following: (1) limited summer and autumn precipitation-driven inflow events and inferred drier conditions (motif A); (2) frequent summer inflow events and inferred wetter conditions (motif B); and (3) large magnitude summer inflow (flood) events (>880 m^3 s^{-1}; motif C).

Towards a hydroclimate-proxy model for the pre-instrumental era

A link between varve stratigraphy and hydrology provides a foundation for developing a hydroclimate-proxy model for the Lake Ohau outflow site. This model, however, is complicated by a lack of pronounced statistical relationship between varve thickness and hydrology, indicating that important mediating variables are at play in the system which accentuate and/or decouple sediment deposition from sediment flux and transport, and hydroclimatic variables such as precipitation and inflow.

The ability to characterize the hydrologic signal by the general accumulation pattern of the different motifs provides a potentially powerful tool for interpreting a longer sediment sequence. Recognizing sedimentation in Lake Ohau is influenced by a range of processes, the demonstrated link between annual hydrography and sedimentary motif can be used to reconstruct pre-historic hydrology. Specifically, sedimentation patterns preserved in cores from the Outflow can be used to reconstruct the general shape of the annual hydrograph, with different sedimentological packages changing in response changes in summer and autumn hydrologic regimes. Given that each of the three major motifs are demonstrably different from one another, observed changes in sedimentary motif can be used to infer changes in seasonal event flow, and by extension storm events, experienced at Lake Ohau. Initial examination of the 5.5 m OH6m1c indicates that the range of facies described herein characterizes the majority of downcore sediment stratigraphy. Similar methods to those described here, including motif descriptions and layer-counting methods, will be employed to ensure we capture any pre-historic variations in the system that were not observed in this study of the instrumental era. Future work will also utilize reanalysis data and synoptic typing specific to New Zealand (Kidson 2000) to establish links to the climate system. The potential correlation between synoptic types and hydrology will allow for a more comprehensive interpretation of the hydroclimatic signal preserved in the Lake Ohau sedimentary sequence.

Conclusions

We have assessed the utility of sedimentary facies of different varve motifs from Lake Ohau to develop a hydroclimate-proxy model which links stratigraphy to the shape of the annual hydrograph. Few robust correlations result from our comprehensive statistical tests of the relationship between varve thicknesses and measured and modeled hydroclimatic variables such as precipitation and inflow at Lake Ohau. Varve thickness is a poor climate proxy at this site, due to the complex interplay between sediment flux and internal lake sediment transport processes. Seasonal thermal stratification, as documented by Roop et al. (2015), has a major influence on sediment accumulation throughout Lake Ohau.

Despite the lack of clear relationships between varve thickness and hydroclimate, there is a quantitative relationship between sediment stratigraphy and summer and autumn inflow patterns. Three primary lamination types presented here represent years with:

(1) limited summer and autumn precipitation-driven inflow events (motif A); (2) frequent summer inflow events (B); and (3) large magnitude summer inflow (flood) events (>880 $m^3 s^{-1}$; C). These relationships provide a tool for characterizing hydrologic variability and storm event frequency for the longer pre-instrumental period. The method used here to compare hydrology and sedimentary facies may be of use for investigating and developing climate-proxy models from other sites where it is difficult to quantitatively link varve thickness and hydroclimatic variability. Overall, this work provides a solid foundation for the development of the Lake Ohau paleoclimate record and is a step towards addressing the current paucity of high-resolution terrestrial paleoclimate reconstructions from the Southern Hemisphere mid-latitudes.

Acknowledgments Financial support was provided through the GNS Science Global Change through Time Program, Sarah Beanland Memorial Scholarship, ANZICE Program (VICX0704), Royal Society of New Zealand Marsden Fund (GNS1302), and KOPRI Project #PP15010. Thanks to Brian Anderson, Lionel Carter, Andrew Lorrey, Christian Ohlendorf and Peter Neff for numerous scientific discussions and ongoing interest in the Lake Ohau Project. We would like to thank the staff at Meridian Energy Ltd. and the University of Otago Marine Sciences Department for logistical support and two anonymous reviewers whose feedback greatly improved the manuscript. Sincere thanks to Chris and Rae Spiers for their hospitality and large workspace at the Killin Barn, and the Inkersell family at Lake Ohau Station for land access and continuing project support.

References

Anderton P (1973) The significance of perennial snow and ice to the water resources of the South Island, New Zealand. J Hydrol 2:6–18

Augustinus P, D'costa D, Deng Y, Hagg J, Shane P (2011) A multi-proxy record of changing environments from ca. 30,000 to 9000 cal. a BP: onepoto maar palaeolake, Auckland, New Zealand. J Quat Sci 26:389–401

Blott SJ, Pye K (2001) GRADISTAT: a grain size distribution and statistics package for the analysis of unconsolidated sediments. Earth Surf Process Landf 26:1237–1248

Bradley RS (1999) Paleoclimatology: reconstructing climates of the Quaternary. Accessed Online via *Elsevier* 68: 1-613

Chater AM, Sturman AP (1998) Atmospheric conditions influencing the spillover of rainfall to lee of the Southern Alps, New Zealand. Int J Climatol 18:77–92

Chutko KJ, Lamoureux SF (2008) Identification of coherent links between interannual sedimentary structures and daily meteorological observations in Arctic proglacial lacustrine varves: potentials and limitations. Can J Earth Sci 45:1–13

Clark MP, Rupp DE, Woods RA, Zheng X, Ibbitt RP, Slater AG, Schmidt J, Uddstrom MJ (2008) Hydrological data assimilation with the ensemble Kalman filter: use of streamflow observations to update states in a distributed hydrological model. Adv Water Resour 31:1309–1324

Cockburn JM, Lamoureux SF (2008) Inflow and lake controls on short-term mass accumulation and sedimentary particle size in a High Arctic lake: implications for interpreting varved lacustrine sedimentary records. J Paleolimnol 40:923–942

Cook ER, Palmer JG, D'Arrigo RD (2002) Evidence for a 'Medieval Warm Period' in a 1100 year tree-ring reconstruction of past austral summer temperatures in New Zealand. Geophys Res Lett 29(14):12–21

Cook ER, Buckley BM, Palmer JG, Fenwick P, Peterson MJ, Boswijk G, Fowler A (2006) Millennia-long tree-ring records from Tasmania and New Zealand: a basis for modelling climate variability and forcing, past, present and future. J Quat Sci 21(7):689–699

Cox S and Barrel D (2007) Geology of the Aoraki area. Institute of Geological and Nuclear Sciences 1:250000 Geological Map, Lower Hutt, New Zealand (GNS Science) vol 71, p 1

Dadson SJ, Hovius N, Chen H, Dade WB, Lin JC, Hsu ML, Lin CW, Horng MJ, Chen TC, Milliman J, Stark CP (2004) Earthquake-triggered increase in sediment delivery from an active mountain belt. Geology 32(8):733–736

Desloges JR, Gilbert R (1994) Sediment source and hydroclimatic inferences from glacial lake sediments: the postglacial sedimentary record of Lillooet Lake, British Columbia. J Hydrol 159:375–393

Doughty AM, Anderson BM, Mackintosh AN, Kaplan M, Vandergoes MJ, Barrell D, Denton GH, Schaefer JM, Chinn TJH, Putnam AE (2013) Evaluation of Lateglacial temperatures in the Southern Alps of New Zealand based on glacier modelling at Irishman Stream, Ben Ohau Range. Quat Sci Rev 74:160–169

Favaro EA, Lamoureux SF (2014) Antecedent controls on rainfall runoff response and sediment transport in a high arctic catchment. Geografiska Annaler Ser A Phys Geogr 96:433–446

Fowler AM, Boswijk G, Lorrey AM, Gergis J, Pirie M, McCloskey S, Palmer JG, Wunder J (2012) Multi-centennial tree-ring record of ENSO-related activity in New Zealand. Nat Clim Chang 2(3):172–176

Hannah DM, Gurnell AM, McGregor GR (2000) Spatio–temporal variation in microclimate, the surface energy balance and ablation over a cirque glacier. Int J Climatol 20(7):733–758

Hicks DM, Shankar U, McKerchar AI, Basher L, Lynn I, Page M, Jessen M (2011) Suspended sediment yields from New Zealand rivers. J Hydrol 50:81–142

Hodder KR, Gilbert R, Desloges JR (2007) Glaciolacustrine varved sediment as an alpine hydroclimatic proxy. J Paleolimnol 38(3):365–394

Horowitz AJ (2003) An evaluation of sediment rating curves for estimating suspended sediment concentrations for subsequent flux calculations. Hydrol Process 17:3387–3409

Howarth JD, Fitzsimons SJ, Norris RJ, Jacobsen GE (2012) Lake sediments record cycles of sediment driven by large earthquakes on the Alpine Fault, New Zealand. Geology 40:1091–1094

Kaufman CA, Lamoureux SF, Kaufman DS (2011) Long-term river discharge and multidecadal climate variability inferred from varved sediments, southwest Alaska. Quat Res 76(1):1–9

Kerr T (2013) The contribution of snowmelt to the rivers of the South Island, New Zealand. J Hydrol 52(2):61–82

Kidson JW (2000) An analysis of New Zealand synoptic types and their use in defining weather regimes. Int J Climatol 20(3):299–316

Lamoureux SF (1994) Embedding unfrozen lake sediments for thin section preparation. J Paleolimnol 10:141–146

Lamoureux SF, Francus P (2014) Layers within layers: quantifying seasonal versus event processes in Arctic clastic varved sediments. Past Global Changes Mag 22(1):6–7

Lorrey AM, Williams P, Salinger J, Martin T, Palmer J, Fowler A, Zhao J, Neil H (2008) Speleothem stable isotope records interpreted within a multi-proxy framework and implications for New Zealand palaeoclimate reconstruction. Quat Int 187(1):52–75

Mackereth FJH (1958) A portable core sampler for lake deposits. Limnol Oceanogr 3:181–191

Mann ME, Zhang Z, Hughes MK, Bradley RS, Miller SK, Rutherford S, Ni F (2008) Proxy-based reconstructions of hemispheric and global surface temperature variations over the past two millennia. Proc Nat Acad Sci USA 105(36):13252–13257

Nash J, Sutcliffe JV (1970) River flow forecasting through conceptual models part I—a discussion of principles. J Hydrol 10(3):282–290

Neukom R, Gergis J (2012) Southern Hemisphere high-resolution palaeoclimate records of the last 2000 years. Holocene 22(5):501–524

Ojala AEK, Francus P, Zolitschka B, Besonen M, Lamoureux SF (2012) Characteristics of sedimentary varve chronologies: a review. Quat Sci Rev 43:45–60

Orpin AR, Carter L, Page MJ, Cochran UA, Trustrum NA, Gomez B, Midenhall DC, Rogers KM, Brackely HL, Northcote L (2010) Holocene sedimentary record from Lake Tutira: a template for upland watershed erosion proximal to the Waipaoa Sedimentary System, northeastern New Zealand. Mar Geol 270(1):11–29

Orwin JF, Smart CC (2004) Short-term spatial and temporal patterns of suspended sediment transfer in proglacial channels, Small River Glacier, Canada. Hydrol Process 18(9):1521–1542

Page MJ, Trustrum NA, DeRose RC (1994) A high resolution record of storm-induced erosion from lake sediments, New Zealand. J Paleolimnol 11:333–348

Page M, Trustrum N, Orpin A, Carter L, Gomez B, Cochran U, Mildenhall D, Rogers K, Brackley H, Palmer A (2010) Storm frequency and magnitude in response to Holocene climate variability, Lake Tutira, North-Eastern New Zealand. Mar Geol 270:30–44

Pharo CH, Carmack EC (1979) Sedimentation processes in a short residence-time intermontane lake, Kamloops Lake, British Columbia. Sedimentology 26(4):523–541

Putnam AE, Schaefer JM, Denton GH, Barrell DJ, Birkel SD, Andersen BG, Kaplan MR, Finkel RC, Schwartz R, Doughty AM (2013) the last glacial maximum at 44 S documented by a 10 Be moraine chronology at Lake Ohau, Southern Alps of New Zealand. Quat Sci Rev 62:114–141

Roop HA, Dunbar GB, Levy R, Vandergoes MJ, Forrest AL, Walker SL, Upton P, Whinney J (2015) Seasonal controls on sediment transport and deposition in Lake Ohau, South Island, New Zealand: implications for a high-resolution Holocene palaeoclimate reconstruction. Sedimentology 62(3):826–844

Sawada M, Johnson PG (2000) Hydrometeorology, suspended sediment and conductivity in a large glacierized basin, Slims River, Yukon Territory, Canada (1993-94). Arctic 53:101–117

Schneider CA, Rasband WS, Eliceiri KW (2012) NIH Image to ImageJ: 25 years of image analysis. Nat Methods 9(7):671–675

Stockhecke M, Anselmetti FS, Meydan AF, Odermatt D, Sturm M (2012) The annual particle cycle in Lake Van (Turkey). Palaeogeogr Palaeoclimatol Palaeoecol 333:148–159

Striewski B, Shulmeister J, Augustinus PC, Soderholm J (2013) Late Holocene climate variability from Lake Pupuke maar, Auckland, New Zealand. Quat Sci Rev 77:46–54

Tait A, Henderson R, Turner R, Zheng X (2006) Thin plate smoothing spline interpolation of daily rainfall for New Zealand using a climatological rainfall surface. Int J Climatol 26(14):2097–2115

Tomkins JD, Lamoureux SF (2005) Multiple hydroclimatic controls over recent sedimentation in proglacial Mirror Lake, southern Selwyn Mountains, Northwest Territories. Can J Earth Sci 42(9):1589–1599

UNSCEAR Annex C (2000) Exposures to the public from man-made sources of radiation. Sourc Eff Ioniz Radiat Sourc UNSCEAR 1:158–287

Walling DE and Webb BW (1988) The reliability of rating curve estimates of suspended sediment yield: some further comments. Sediment Budgets, IAHS Publ 174

Wheatley JJ, Blackwell PG, Abram NJ, McConnell JR, Thomas ER, Wolff EW (2012) Automated ice-core layer-counting with strong univariate signals. Clim Past 8:1869–1879

Woods R, Hendricks J, Henderson R, Tait A (2006) Estimating mean flow of New Zealand rivers. J Hydrol 45(2):95–109

Zolitschka B, Pike J (2014) Maximizing the information yield from annually resolving natural archives. Past Global Changes Mag 22(1):4–5